Dispersion of absorption and refractive index of PbTe and $Pb_{1-x}Eu_xTe$ ($x < 0.05$) below and above the fundamental gap

Shu Yuan, H. Krenn, G. Springholz, and G. Bauer
Institut für Halbleiterphysik, Johannes Kepler Universität Linz, A-4040 Linz, Austria
(Received 17 September 1992; revised manuscript received 30 November 1992)

We report extensive experimental and theoretical studies of the frequency dependence of the absorption constant $\alpha(\omega)$ and of the index of refraction $n(\omega)$ in PbTe and its pseudobinary alloy $Pb_{1-x}Eu_xTe$. Mid-infrared transmission experiments on epitaxial layers of $Pb_{1-x}Eu_xTe$ ($0 \le x \le 0.0475$, thickness ≈ 5 μm) on BaF_2 substrate were performed in the frequency range 1000–5000 cm^{-1} at temperatures from 5 to 300 K. The absolute values of the transmission as a function of frequency can be evaluated to yield information on both $\alpha(\omega)$ and $n(\omega)$, due to the presence of interference fringes below the fundamental energy gap and due to the drop of transmission above the energy gap. For $\alpha(\omega)$ a model calculation is preferred based on the nonparabolic Dimmock model for the energy-momentum relationship $\epsilon(\mathbf{k})$ of electrons and holes. For the oscillator strength, interband matrix elements $P_{\parallel}$ and $P_{\perp}$ are used that are in agreement with the values obtained from magneto-optical studies. In the procedure to fit the transmission spectra four parameters are used: energy gap, oscillator strength, damping parameter, and a background index of refraction. With these parameters the functional dependence $\alpha(\omega)$ is calculated, and $n(\omega)$ is derived using a Kramers-Kronig transformation. The results show that nonparabolicity is quite important to reproduce $\alpha(\omega)$, and that via Kramers-Kronig transformation it also substantially influences $n(\omega)$. Through the causality relation, even for frequencies below that corresponding to the energy gap, $n(\omega)$ is influenced by the shape of $\epsilon(\mathbf{k})$ above the gap. With increasing Eu content the energy gap increases and the extremum in $n(\omega)$ close to ϵ_g shifts to higher energies. The enhancement over the background refraction index, which is determined by higher interband transitions, becomes weaker. For Eu contents $x \approx 0.05$ the oscillator strength increases by about 10% in comparison to PbTe. In addition, the damping parameters increase from 3 to 40 cm^{-1} at $T = 5$ K.

I. INTRODUCTION

Presently, there is again much interest in the optical properties of semiconductors,[1,2] especially in the refractive index of epitaxial layers as well as quantum-well structures. It is important to know the dispersion of the refractive index in the design and analysis of optical filters, of mirrors coated with thin films, and of waveguiding semiconductor devices like semiconductor lasers and modulators. In a wide range of photon energies (from 0 to above 6 eV), optical constants are usually determined by spectroscopic ellipsometry. However, Kim *et al.*[1] suggested that spectroscopic ellipsometry does not measure the true bulk dielectric function. Near the fundamental energy gap, transmission or reflectivity measurements have been commonly used to determine the optical constants of thin films, either by dealing only with the minima and maxima of Fabry-Perot (FP) interferences or by fully analyzing the transmission or reflection spectra. With the aid of the former ones, only the optical constants below the energy gap can be determined. In the analysis of the latter method, an empirical formula is employed to describe the dependence of the absorption coefficient (α) near the energy gap on photon energy. Both approaches usually do not take into account the intrinsic relationship between α and the index of refraction n, i.e., the Kramers-Kronig (KK) relationship. Instead, some empirical relations, like the Cauchy relation[3] and the Sellmeier relation,[2] were used to describe the dispersion of the refractive index n. Therefore, the optical constants determined by such methods are only valid for a narrow range of photon energies. Four effects are found to have a major influence on the optical transmission of epitaxial films:[3] (i) reflection at the substrate-to-air interface, (ii) absorption within the substrate, (iii) interference fringes arising from the epitaxial film layer, (iv) absorption within the epitaxial layer. Since the transmission or reflection spectra of a thin film depend on the absorption coefficient, the refractive index, and the thickness of the film, it is necessary to treat α and n self-consistently through the Kramers-Kronig relation. For layered structures, the common Kramers-Kronig analysis is not directly applicable to the reflectivity spectra, since it is not straightforward to get the phase of reflectivity without mathematical tricks to guarantee causality.[4]

Among the narrow-gap semiconducting compounds, the lead chalcogenides PbS, PbSe, and PbTe and their ternary compounds $Pb_{1-x}Sn_xTe$, $Pb_{1-x}Eu_xTe$, and $Pb_{1-x}Eu_xSe$ play an important role as mid-infrared emitters and detectors in the wavelength range of 3–30 μm.[5,6] The interaction of photons with free and bound carriers in these compounds has a long history of investigation.[7] In the far infrared, the optical response (measured by reflection spectroscopy) is mainly determined by free-carrier absorption and lattice vibrations. Since the

masses of anions and cations in the fcc Bravais lattice are heavy (e.g., Te and Pb), the phonon wavelengths are in the range of about 100 μm and above, i.e., far outside the range of interest for applications in the mid-infrared. Thus from the far infrared toward the fundamental absorption edge[8] ($\hbar\omega \approx \epsilon_g$, where ϵ_g denotes the energy gap) these semiconductors act as high index of refraction materials at moderate extinction coefficients ($n \approx 5-6$, $k \approx 0.01$). Therefore, these compounds are particularly interesting because of their high polarizability in the infrared (which is much higher than that of the elemental semiconductors Si and Ge).

The ternary alloys of IV-VI compounds with magnetic (Mn^{2+}, Eu^{2+}, Gd^{2+}, etc.) and nonmagnetic (Sn^{2+}, Cd^{2+}, Sr^{2+}, etc.) ions[9-11] are of special interest, since for the former, so-called semimagnetic semiconductors, the electronic band-structure properties are drastically influenced by external magnetic fields. For all ternary compounds, the energy gap increases with the content of the substituents, except for PbSn(Te,Se) for which the band alignment of conduction and valence bands is interchanged at certain Sn concentrations.

In our work we will concentrate on $Pb_{1-x}Eu_xTe$ ($x = 0$, 1.9%, 2.65%, and 4.75%), which is of particular relevance for mid-infrared devices. Very low threshold current diode lasers have been obtained in single quantum wells based on the lattice matched $PbTe/Pb_{1-x}Eu_xTe_{1-y}Se_y$ heterojunction ($\lambda > 2.7$ μm for $y = 0$),[12] and PbTe insulated-gate field-effect transistors[13] have been fabricated using a PbTe/EuTe superlattice between the BaF_2 substrate and the PbTe channel (where the velocity of electrons saturates close to the speed of light). So far no data of optical constants are available for the mixed crystals of $Pb_{1-x}Eu_xTe$ over a wide temperature range.

Single crystals of these semiconductors are grown by the Bridgman method, or by hot wall[14] and molecular-beam epitaxy[9] if films on insulating substrates (NaCl, KCl, LiF, and BaF_2) are desired. The density of free carriers can be controlled either by intentional doping, or originates from anion or cation vacancies. The smallness of the effective mass both of electrons and of holes is typical for this group of IV-VI narrow-gap semiconductors and is related to the strong interaction of close-lying valence and conduction bands of symmetry L_6^+, L_6^- at the L point of the Brillouin zone.

The onset of direct interband transitions at the fundamental energy gap was treated by Walton and Moss[15] using a single oscillator at $\lambda_0 = hc/\epsilon_g$ and relating the refractive index $n(\lambda)$ to n_0 of an empty lattice at infinite wavelength:

$$\frac{n_0^2-1}{n^2+1} = 1 - \left[\frac{\lambda_0}{\lambda}\right]^2 . \tag{1}$$

For extrapolation to low frequencies, n_0 can be approximated by the Drude expression including the optic-phonon contribution to the dielectric function.[16] For PbTe a reliable determination of optical constants (at 77 and 300 K) from below band-gap ($\lambda = 5-12$ μm) transmission was given by McCarthy, Weber, and Mikkor[17] in the regime $k^2 \ll (n-1)^2$, $k \approx 0.1$, $n \approx 5-6$, where the extinction coefficient can be obtained from transmission maxima alone. An additional absorption just below the band gap with exponential tails (Urbach tail) was attributed to chlorine contamination in PbTe films deposited on NaCl substrates. Data of n for PbTe for room temperature and 77 K were presented by Zemel, Jensen, and Schoolar,[18] Globus *et al.*[19] and (also for $T = 20$ K) by Piccioli, Beson, and Balkanski.[20] The latter authors pointed out the causality between n and α and its influence on the singularity of the slope of the index of refraction near the absorption edge. To obtain a correct fit to the decreased values of n ($n = 5.8$) below 2000 cm^{-1} and the maximum of n at 2600 cm^{-1} ($T = 300$ K), Piccioli, Beson, and Balkanski had to take into account explicitly the exponential part of absorption $\alpha(\epsilon)$ below the band gap, and the conjugate Kramers-Kronig pair $n(\epsilon), \alpha(\epsilon)$:

$$n(E) = 1 + \frac{hc}{\pi}\int_0^\infty \frac{\alpha(E')}{E'^2 - E^2} dE' . \tag{2}$$

The dispersion of the index of refraction near the fundamental energy gap is still a point of controversy. The existence of any excitonic absorption may explain a stronger decrease of n above ϵ_g, but this explanation is unlikely in IV-VI compounds due to their huge dielectric constants. In Refs. 21 and 8 two related narrow-gap compounds $Hg_{1-x}Cd_xTe$ and PbTe (Ref. 21) [and $Pb_{1-x}Sn_xTe$ (Ref. 8)] with similar energy gaps were compared with each other. The correlation between the index of refraction maximum near ϵ_g and the slope of the onset of the absorption edge for pseudobinary PbSe narrow-gap semiconductors was emphasized in Ref. 22.

In the photon energy range $\epsilon \gg \epsilon_g$, the absorption coefficient α depends on the special features of the energy bands close to the ones at the L point of the Brillouin zone. PbTe has at least one additional series of valence-band extrema in the $\langle 100 \rangle$ directions (Σ points of the Brillouin zone). Due to these additional extrema along the Σ and Λ directions, the absorption spectra exhibit steps at $\epsilon = 1.45$ and 2.6 eV for room temperature.[19,23,24] Nonparabolicity and the occurrence of various Van-Hove singularities in the energy band scheme were taken into account, however, not primarily for the evaluation of the optical constants (n, κ) near the fundamental energy gap. Greenaway and Cardona[25] have found good correspondence of oscillator fits to measurements at higher energies in the absorption regime $\epsilon \gg \epsilon_g$ ($\epsilon = 1-17$ eV) without showing the validity of the fit in the absorption range near ϵ_g. The harmonic-oscillator model[26] does not incorporate the concept of an optical energy band gap ϵ_g. Thus, the optical energy band gap of semiconductors and dielectrics cannot be directly determined from this approach. Furthermore, many fitting parameters are needed to describe the optical constants in the fundamental gap range.

The precise knowledge of optical constants (and absorption coefficient α) above and below the fundamental absorption edge is particularly important for the investigation of layered systems consisting of IV-VI semiconductors (for coatings[27] or nowadays for multilayers[5,28] of

different IV-VI compounds). Without such information, no fit to reflectance and transmittance spectra over a wide range of photon energies is possible from the low to high absorbing regions. It is the purpose of this work to find reliable data for the optical constants.

We present a model that yields excellent fits to experimental transmission spectra of PbTe and $Pb_{1-x}Eu_xTe$ epilayers over a wide temperature range (5, 77, and 295 K). For PbTe the resulting absorption coefficient and refractive index are in excellent agreement with published data. So far, there are no data available for $Pb_{1-x}Eu_xTe$, $x \leq 0.05$.

The paper is organized as follows. In Sec. II transmission spectra of a high-quality epitaxial PbTe layer and three $Pb_{1-x}Eu_xTe$ layers (x =0.019, 0.0265, and 0.0475) at temperatures 5, 77, and 295 K are presented and compared with model fits. The optical constants are evaluated in Sec. III, starting from the calculation of the optical dielectric function using a *nonparabolic two-band-model*. Lifetime broadening[29] of the energy levels is included. The momentum conservation between the absorbed photon and the excited electron, which is stringent for crystalline solids of translation symmetry, is strictly fulfilled in our calculations. In Ref. 29, the expression for the absorption coefficient was taken from a treatment of amorphous solids for calculating $\alpha(\omega)$ in crystalline solids, but this violates momentum conservation. We include the requirement of momentum conservation into the method described in Ref. 29 and expand it to the case of nonparabolic energy bands in a narrow-gap semiconductor. A Kramers-Kronig transformation is applied to find the index of refraction from the calculated extinction coefficient. The set of essential fitting parameters is reduced to four: (i) energy gap, (ii) oscillator strength, (iii) lifetime broadening, and (iv) background index of refraction. The negative dispersion of the index of refraction slightly above the energy gap is evaluated in context of nonparabolic energy bands. From the results (Sec. IV), the interband matrix elements and oscillator strengths are extracted from the two-band model and from the comparison to transmission spectra. The peculiarities of near-band-gap optical properties of lead salts are discussed in Sec. V in comparison to other narrow-gap semiconductors. The validity of the nonparabolic two-band model for the description of optical absorption above and below the band gap follows from a comparison to the experimental data.

II. EXPERIMENTS

The samples under investigation are (111)-oriented epitaxial layers on insulating substrates (BaF_2). They were grown by molecular-beam epitaxy (MBE) under ultrahigh-vacuum conditions.[30] The PbTe, Eu, and Te_2 beam flux rates from the effusion cells were measured by a crystal thickness monitor and adjusted for a growth rate of 1.1 μm/h and for the desired x content of the $Pb_{1-x}Eu_xTe$ layers. The sample parameters are given in Table I. Sample *A* is the binary compound PbTe. Samples *B*, *C*, and *D* are ternary compounds $Pb_{1-x}Eu_xTe$ with varying x contents from x =0.019 to 0.0475. The nominal Eu content x was extracted from the measured energy gap at 5 K by using the expression of Partin:[5] $\epsilon_g(x, T \rightarrow 4.2\ \text{K}) = 187\ \text{meV} + x \cdot 6000\ \text{meV}$, and the ultimate accuracy was ± 2 meV (at T =5 K) for the determination of the energy gap from fits to transmission spectra. The electric transport properties, Eu contents, and film thicknesses are given in the left part of Table I. For the samples *B* (x =0.019) and *C* (x =0.0265) the Te_2 to Eu beam flux ratio was about 1.2, for sample *D* (x =0.0475) about 1.8. The monatomic layer-by-layer growth was monitored by *in situ* reflection high-energy electron diffraction (RHEED).[30] The film thicknesses of 3.9–4.5 μm are sufficient for complete strain relaxation with respect to the substrate. Thus the samples behave like bulk crystals, and strain-induced effects on the electronic band-structure properties (symmetry, splittings) can be excluded.

The relatively large optical thickness of the samples enables us to observe a sufficient number of Fabry-Perot fringes in the transmission range below the fundamental gap. In our case the peak-to-valley ratio of the FP fringes proves the high optical finesse of the epitaxial film samples.

TABLE I. Electric transport and optical parameters of $Pb_{1-x}Eu_xTe$ epitaxial layers on BaF_2.

Sample	x	d (μm)	T (K)	N (10^{16} cm^{-3})	μ (cm^2/V s)	ϵ_g (meV)	B	Γ (cm^{-1})	n_∞
A	0	4.5	295	−6.2	500	319	0.54	18	5.67
			77	−1.6	19 700	211 213[b]	0.57	3	6.00
			5	−0.6[a]	465 000[a]	190 190[b]	0.56	3	6.07
B	0.019	4.0	295			396	0.54	30	5.33
			77	−1.1	3080	324	0.57	10	5.53
			5			302	0.51	5	5.60
C	0.0265	4.8	295	+8.4	165	441	0.49	10	5.13
			77	+5.9	1790	359	0.52	10	5.31
			5			347	0.53	10	5.34
D	0.0475	3.9	295	−2.0	52	541	0.57	50	4.82
			77	−2.3	832	481	0.60	35	4.94
			5			472	0.62	40	4.96

[a]For T =20 K.

[b]ϵ_g determined from the onset of PC spectra; see Figs. 3(b) and 3(c).

The transmission measurements were performed by mounting the sample in a variable-temperature optical cryostat (ZnSe windows) on a proper sample holder which can be lifted up and down to expose either the sample or a reference diaphragm (a hole or the BaF_2 reference sample) to the beam. The absorption in the BaF_2 substrate was eliminated by normalizing the transmission of the sample to a bare BaF_2 substrate with the same thickness.

The cryostat is inserted in the interferometer chamber of a Bruker IFS-113v Fourier-transform spectrometer. The spectral resolution is 4 cm^{-1} and the photometric accuracy is better than 1% over the full wave-number range from 1000 to 4000 cm^{-1}. The additive noise-limited sensitivity is especially important to recover spectral features in the strong absorbing regime above the fundamental absorption edge.

In Fig. 1, the transmission of the PbTe sample A versus frequency divided by that of its BaF_2 substrate is shown for the temperatures $T=295$, 77, and 5 K together with model fits (solid curve, nonparabolic two-band model; dashed curve, parabolic limit of the two-band model). The most obvious influence of the temperature variation on the transmission spectra is the shift of the fundamental absorption edge to higher photon energies with increasing temperature. From Fig. 1(a) it can be seen that the nonparabolic model fits the experimental data much better than the parabolic one using the same band parameters. In Figs. 1(b) and 1(c) only the fits for the nonparabolic two-band model are included.

Figures 2(a)–2(c) show transmission spectra for three ternary compounds $Pb_{1-x}Eu_xTe$ at $T=5$ K. The fundamental absorption is shifted to higher frequencies with increasing Eu content. By comparison of Fig. 2(c) to the spectrum of the PbTe sample [Fig. 1(c)], one recognizes a stronger absorption below the energy gap ϵ_g over a broader photon energy range than that observed for PbTe. We believe that enhanced absorption due to alloy fluctuations is responsible for this behavior.

The transmission spectra of $Pb_{1-x}Eu_xTe$ ($x=0.019$, 0.0265, and 0.0475) at temperatures $T=77$ and 295 K were also measured and included in the analysis of the data (Sec. IV). They are not shown in separate plots for brevity.

III. DERIVATION OF OPTICAL CONSTANTS FOR NONPARABOLIC INTERBAND TRANSITIONS

In order to reduce the number of parameters for fitting spectra, only interband transitions close to the fundamental energy gap (L_6^+, L_6^-) in PbTe and $Pb_{1-x}Eu_xTe$ are considered. Contributions due to free-carrier absorption and lattice vibrations (as well as from critical points above the fundamental energy gap) are neglected. Thus for near-fundamental absorption we use a simple two-band model with a nonparabolic energy-momentum relation according to Dimmock and Wright[31] or Mitchell and Wallis[32] (neglecting the contributions from the far bands) with a pair of interband matrix elements $P_\parallel, P_\perp$ which describe the strong nonspherical anisotropy of the conduction and valence bands at the L point of the Brillouin zone. The energy gap ϵ_g is modified according to the Eu content in the ternary compound $Pb_{1-x}Eu_xTe$, and its temperature dependence is taken into account as well. The dispersion relationship is given by

$$\epsilon_c(\mathbf{k})=\frac{\hbar^2}{2m_0}\mathbf{k}^2+\frac{1}{2m_0}[4\hbar^2P_\perp^2(k_x^2+k_y^2)+4\hbar^2P_\parallel^2k_z^2+m_0^2\epsilon_g^2]^{1/2}, \quad (3)$$

$$\epsilon_v(\mathbf{k})=\frac{\hbar^2}{2m_0}\mathbf{k}^2-\frac{1}{2m_0}[4\hbar^2P_\perp^2(k_x^2+k_y^2)+4\hbar^2P_\parallel^2k_z^2+m_0^2\epsilon_g^2]^{1/2}. \quad (4)$$

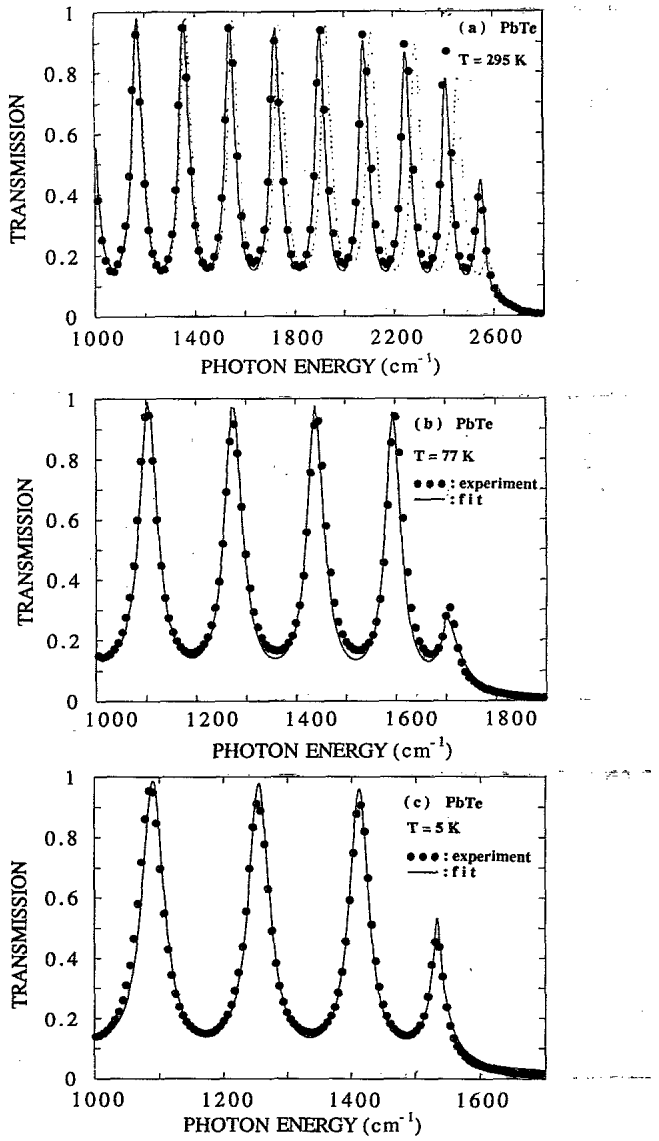

FIG. 1. Transmission spectra of a 4.5-μm epitaxial layer PbTe on BaF_2, sample A, for various temperatures: (a) 295 K, (b) 77 K, (c) 5 K. The solid and dashed lines are model fits: the best agreement with experimental data (circles) is obtained by using the nonparabolic two-band model (solid lines), whereas in the limit of a parabolic two-band model (with identical band-edge masses) the phase of Fabry-Perot interferences does not fit the measurements as shown in (a).

The z axis is parallel to a [111] direction, i.e., perpendicular to the Brillouin-zone boundary at the L point, and m_0 is the free-electron mass. The zero energy is chosen to be in the middle of the forbidden gap ϵ_g. In the strict two-band model, both the conduction and valence bands are mirrorlike in the ϵ versus $\mathbf{k}$ dependence, since far-band contributions are not taken into account. The momentum matrix elements $P_\parallel$ and $P_\perp$ differ considerably for interband transitions parallel and perpendicular to the principal axes of the energy ellipsoid in the $\mathbf{k}$ space. They are related to the anisotropic band-edge masses $m_\parallel$ and $m_\perp$ at the L point of the Brillouin zone:[31]

$$\frac{2P_\perp^2}{m_0}=\epsilon_g\frac{m_0}{m_\perp}\ ,\quad \frac{2P_\parallel^2}{m_0}=\epsilon_g\frac{m_0}{m_\parallel}\ . \tag{5}$$

Since it is well known that the far bands modify the effective masses of electrons and holes by up to 30%, the corrected values quoted in Eq. (5) do not correspond to these which are obtained from fits to magneto-optical experiments using both the exact conduction-band–valence-band interaction and considering the effect of the far bands in the k^2 approximation.[32] For the calculation of the absorption coefficient we modify the two-band parameters $P_\parallel$ and $P_\perp$ so as to result approximately in the proper mean electron and hole mass anisotropy and to also yield proper mean values of the transverse ($m_\perp$) and longitudinal ($m_\parallel$) effective masses. Up to about $x=0.05$ the band alignment of $Pb_{1-x}Eu_xTe$ does not change,[5,33] and $P_\perp$ and $P_\parallel$ are assumed to be constant, i.e., independent of x.

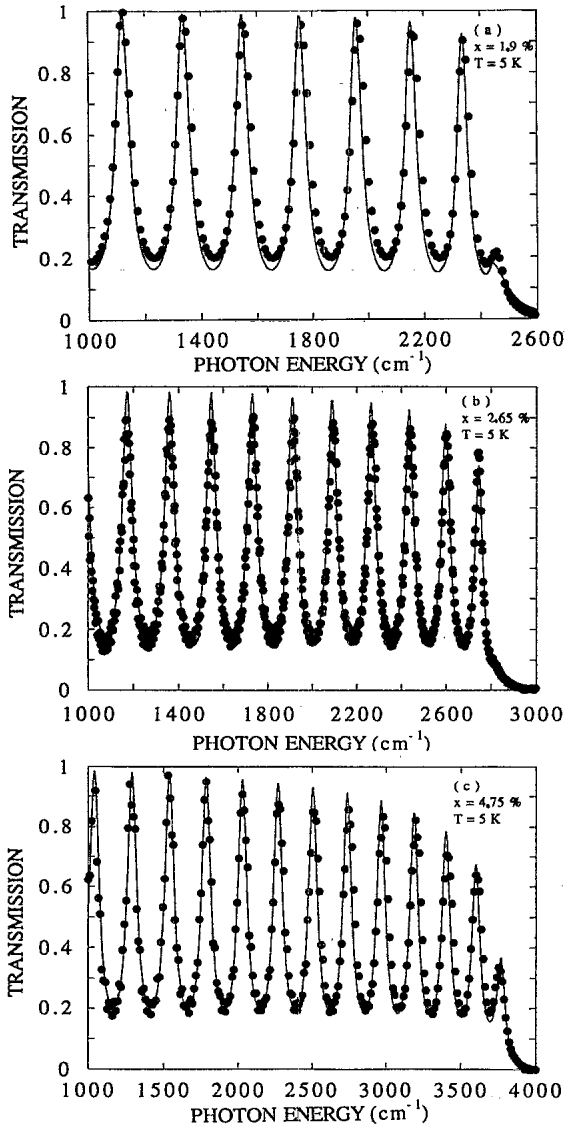

FIG. 2. Transmission spectra of $Pb_{1-x}Eu_xTe$ epitaxial layers on BaF_2 at $T=5$ K for various Eu contents: (a) sample B, $x=0.019$; (b) sample C, $x=0.0265$; (c) sample D, $x=0.0475$. The solid lines are model fits according to the nonparabolic two-band model.

The joint density of states $J_{cv}(\epsilon)$ for an optical transition $\epsilon=\hbar\omega=\epsilon_c(\mathbf{k})-\epsilon_v(\mathbf{k})$ is derived (see Appendix A) from Eqs. (3) and (4) and is given by

$$J_{cv}(\epsilon)=\frac{m_0^3}{8\pi^2\hbar^3P_\perp^2P_\parallel}\epsilon(\epsilon^2-\epsilon_g^2)^{1/2}\ . \tag{6}$$

In the parabolic limit, $\epsilon\approx\epsilon_g$, Eq. (6) can be simplified to the usual square-root-like joint density of states for parabolic energy bands:

$$J_{cv}^{(p)}(\epsilon)=\frac{\sqrt{2}m_0^3}{8\pi^2\hbar^3P_\perp^2P_\parallel}\epsilon_g^{3/2}\sqrt{\epsilon-\epsilon_g}\ . \tag{7}$$

The optical dielectric function is identical with the longitudinal dielectric function of Lindhart in the limit $\mathbf{q}\to0$, except that the direction of the momentum is in the direction of the electric field of the light wave [see formula (2.9) of Ref. 1]:

$$\hat{\epsilon}(\omega)=1-\frac{\hbar^2e^2}{m_0^2\epsilon_0}\sum_{c,v}\int J_{cv}(\epsilon')d\epsilon'\frac{|\mathbf{e}\cdot\mathbf{p}_{cv}(\epsilon')|^2}{\epsilon'^2}\times\left[\frac{1}{\hbar\omega-\epsilon'+i\Gamma}-\frac{1}{\hbar\omega+\epsilon'+i\Gamma}\right]\ . \tag{8}$$

$\mathbf{p}_{cv}$ is the energy-dependent electric-dipole matrix element in the momentum representation which enters in first-order perturbation as interaction of the light wave (polarization unit vector $\mathbf{e}$) with the carriers in the valence and conduction bands (e is the electron charge, and ϵ_0 is the permittivity of free space). Due to defect scattering, electron-phonon scattering, electron-electron scattering, alloy scattering, etc., the linewidth is finite and introduced into Eq. (8) by a "broadening" parameter Γ. Equation (8) is readily a special case for Γ being a constant which describes a Lorentzian line-shape broadening of the electronic states.[1] Since the semiconductors which we investigate (PbTe and $Pb_{1-x}Eu_xTe$) are valley degenerate at the L point of the Brillouin zone corresponding to the various $\langle 111\rangle$ directions, the average square of the interband transition matrix elements is evaluated in Appendix B for the longitudinal valley parallel [111] with $\mathbf{e}\perp[111]$ and for the three equivalent valleys $[\bar{1}11]$, $[1\bar{1}1]$, and $[11\bar{1}]$ which are oblique to $\mathbf{e}$. The result is[8]

$$\langle |\mathbf{e}\cdot\mathbf{p}_{cv}(0)|^2\rangle_{\text{valleys}}=\tfrac{8}{3}(\mathbf{P}_{\parallel}^2+2\mathbf{P}_{\perp}^2)\ . \tag{9}$$

From Eq. (8) one can separate the real and imaginary parts of the optical dielectric function, and evaluate the optical constants without additional assumptions, for which two integrals have to be calculated. We shall follow an alternative way: in a first stage, an analytical expression for the (simpler) imaginary part of the dielectric function is derived which can be presented in an analytical form for Lorentzian line-shape broadening. With a little loss of generality (through the assumption of an average index of refraction $\langle n\rangle$), the absorption coefficient is obtained. Finally, a numerically much more convenient Kramers-Kronig transformation yields the index of refraction. By that procedure, the causality between the optical constants is obeyed.

Neglecting the second term in the large parentheses of Eq. (8), which is only a small correction to near-band-gap absorption, and keeping the transition matrix element energy independent, the imaginary part of the dielectric function is

$$\mathrm{Im}[\hat{\epsilon}(\omega)]=\frac{\pi\hbar^2e^2\langle |\mathbf{e}\cdot\mathbf{p}_{cv}(0)|^2\rangle_{\text{valleys}}}{m_0^2\epsilon_0}\times\int J_{cv}(\epsilon')\frac{1}{\epsilon'^2}d\epsilon'\frac{\Gamma/\pi}{(\hbar\omega-\epsilon')^2+\Gamma^2}\ . \tag{10}$$

From Eq. (10), the extinction (κ) and absorption coefficient (α) can be derived in the usual way (abbreviating the prefactor prior to the integral as A):

$$\kappa(\omega)=\frac{\mathrm{Im}[\hat{\epsilon}(\omega)]}{2\langle n\rangle}=\frac{A}{2\langle n\rangle}\left[\frac{J_{cv}(\omega)}{(h\omega)^2}\right]\otimes\Gamma(\omega) \tag{11}$$

and

$$\alpha(\omega)=\frac{\omega\,\mathrm{Im}[\hat{\epsilon}(\omega)]}{c_0\langle n\rangle}=\frac{\omega A}{c_0\langle n\rangle}\left[\frac{J_{cv}(\omega)}{(h\omega)^2}\right]\otimes\Gamma(\omega)\ . \tag{12}$$

The integral of Eq. (10) is generalized as a convolution of $J_{cv}(\omega)/(\hbar\omega)^2$ with the Lorentzian broadening function $\Gamma(\omega)$:

$$\Gamma(\omega)=\frac{\Gamma/\pi}{(\hbar\omega)^2+\Gamma^2}\ . \tag{13}$$

The convoluting operator ($\otimes$) between a function $f(\omega)$ and $\Gamma(\omega)$ is defined as usual:

$$f(\omega)\otimes\Gamma(\omega)=\int f(\epsilon)\Gamma(\omega-\epsilon)d\epsilon\ . \tag{14}$$

Equation (12) is more general than the initial integral Eq. (10), since it is not restricted to Lorentzian broadening. It can be formally applied also to lower-dimensional structures such as quantum wells, quantum wires, and quantum dots.[34]

To relate the theory to fits of experimental data, Eq. (6) is explicitly inserted into Eq. (11), and all constant parameters are taken together in a common constant B, which is accessible to a determination from measurements:

$$\kappa(\omega)=B\int_{\epsilon_g}^{\infty}\frac{(\epsilon'^2-\epsilon_g^2)^{1/2}}{\epsilon'}\frac{\Gamma/\pi}{(\hbar\omega-\epsilon')^2+\Gamma^2}d\epsilon'\ , \tag{15}$$

$$B=\frac{e^2m_0(\mathbf{P}_{\parallel}^2+2\mathbf{P}_{\perp}^2)}{3\pi h\langle n\rangle\epsilon_0\mathbf{P}_{\parallel}\mathbf{P}_{\perp}^2}\ . \tag{16}$$

In the parabolic limit $\hbar\omega\approx\epsilon_g$, the convolution integral Eq. (11) can be expressed in analytic form, using the joint density of states of Eq. (7):[34]

$$\kappa^{(p)}(\omega)=B^*\frac{1}{(h\omega)^2}\frac{\Gamma}{\{[(h\omega-\epsilon_g)^2+\Gamma^2]^{1/2}-(h\omega-\epsilon_g)\}^{1/2}}\ , \tag{17}$$

$$B^*=\frac{\sqrt{2}e^2m_0(\mathbf{P}_{\parallel}^2+2\mathbf{P}_{\perp}^2)}{3\pi h\langle n\rangle\epsilon_0\mathbf{P}_{\parallel}\mathbf{P}_{\perp}^2}\epsilon_g^{3/2}\ . \tag{18}$$

At this point, a discrepancy of Eq. (17) to Eq. (15) of Ref. 29 for $\kappa(\epsilon)$ is obvious. In Ref. 29, for crystalline solids, $\kappa(\epsilon)=(\epsilon-\epsilon_g)^2A/(\epsilon^2-B\epsilon+C)$ was derived at a certain critical point. The disagreement comes about from (i) replacing the convolution Eq. (11) by a simple multiplication with $\Gamma(\epsilon)=A/(\epsilon^2-B\epsilon+C)$, and (ii) by using a functional form for the joint density of states $J_{cv}=(\epsilon-\epsilon_g)^2$ which violates the momentum conservation. If δ-like absorption at certain critical points is assumed, statement (i) can be justified, but it becomes increasingly wrong for interband transitions continuously distributed over a wider dispersion regime. The latter takes place especially near the M_0 critical point for the fundamental absorption regime. Statement (ii) comes from the derivation of density of states in amorphous solids, which must not obey any momentum conservation.

Near the fundamental absorption edge (M_0), the full nonparabolic dispersion of the participating energy bands is considered. The Kramers-Kronig relationship yields the energy dependence of the index of refraction:[29]

$$n(\epsilon)=n_{\infty}+\frac{1}{\pi}P\int_{-\infty}^{+\infty}\frac{\kappa(\epsilon')-\kappa_{\infty}}{\epsilon'-\epsilon}d\epsilon'\ . \tag{19}$$

The Kramers-Kronig transformation of the extinction coefficient at the critical points above the fundamental energy gap (apart from M_0) also contributes to the refractive index near and below the energy gap. It is related to absorptions at critical points M_j ($j\neq 0$) apart from the fundamental L point at higher energies.

After the complex index of refraction $n+i\kappa$ is determined by calculation, the transmission through an epitaxial layer grown on an insulating substrate (BaF_2) can be evaluated using a transfer-matrix method. The method developed in Ref. 35 was applied to our two-layer system. The optical constants n_f and κ_f of the film are taken from Eqs. (15) and (19), and the substrate (BaF_2) is assumed to be nonabsorbing in the frequency range of interest. The refractive index of BaF_2 is taken as $n_s=1.39$ for all three temperatures 5, 77, and 295 K. It was determined from the FP fringes of a thin bare BaF_2 plate in the frequency region 100–4000 cm^{-1}. The optical thickness (n_sd_s) of the substrate is so large that constructive

interferences are not observed in our experiments.

In summarizing all parameters which determine the transmission spectra, one ends up with four essential fitting parameters which depend on the electronic band properties: the energy gap ϵ_g, B, which is proportional to the oscillator strength of the interband transition [Eq. (16)], Γ as Lorentzian linewidth, and n_∞ as background index of refraction due to higher critical points [Eq. (19)]. The remaining geometrical parameters are the film thickness (d_f) and the thickness (d_s) of the substrate, which can be determined independently by other methods (depth profiling) and are not regarded as fitting parameters.

IV. RESULTS

Nonparabolicity effects on optical absorption are apparently of essential importance in the narrow-gap semiconductors which we investigated, because the final electronic states of optically excited carriers lie considerably above (for electrons) and below (for holes) the band edges. Assuming symmetric energy bands L_6^- and L_6^+ (as represented by an exact two-band model for PbTe-related compounds), the final carrier energies are comparable to $0.5\epsilon_g$ for $\hbar\omega \leq 2\epsilon_g$ in our fits. Free-carrier and phonon effects can be excluded in this photon energy range, particularly due to screening by the high lattice polarizability and due to the relatively large anion and cation masses. The LO-phonon frequency of PbTe is 114 cm^{-1}; for $Pb_{1-x}Eu_xTe$ it is smaller than 150 cm^{-1} in the range of concentrations $x \leq 0.048$. Thus the LO modes do not contribute to the dielectric function in the frequency range between 1000 and 4000 cm^{-1}. The screened ($\epsilon_\infty \approx 35$) plasma frequency is also below 200 cm^{-1} for carrier concentrations smaller than 10^{17} cm^{-3}. For photon energies considerably higher than $2\epsilon_g$(PbTe), transitions originate from other close-lying valence-band extrema, presumably in the direction of Σ, which can be included in the exact two-band model phenomenologically by setting oscillators near some critical points.[24] If we assume that the nonparabolic two-band model is valid up to the wave-number range of 5000 cm^{-1}, the analysis of the measured transmission data gives the optical constants for both PbTe and $Pb_{1-x}Eu_xTe$ using only four essential fitting parameters, which are given in the right part of Table I.

In order to show the relevance of the nonparabolic energy bands for the interpretation of transmission data close to the fundamental absorption, in Fig. 1(a) two fits are compared with experimental transmission spectra: (i) for parabolic bands (dashed curve), (ii) for nonparabolic bands (solid curve) using the same band parameters. From the difference of both model plots we conclude that the energy-momentum relationship $\epsilon(\mathbf{k})$ *above* the energy gap, which determines $\alpha(\omega)$, in turn influences $n(\omega)$ through the Kramers-Kronig transform also for frequencies *below* the gap energy; i.e., the proper dependence $\alpha(\omega)$ determined by $\epsilon(\mathbf{k})$ *above* the gap energy also determines the quality of the fit to the transmission *below* the gap. Therefore, in the fits of Figs. 1(b) and 1(c) and Figs. 2(a)–2(c) only the nonparabolic $\epsilon(\mathbf{k})$ dispersion was used for calculating the optical constants $n(\omega)$ and $\kappa(\omega)$.

The absorption coefficient α is plotted versus photon energy in Figs. 3(a)–3(c) for three temperatures. The onset of absorption can be also observed in the photoconductivity (PC) spectra which are given in the insets of the Figs. 3(b) and 3(c) for PbTe at temperatures $T = 77$ and 5 K. The energy gaps derived from the PC spectra are in excellent agreement with the onsets of the absorption coefficient as obtained from the transmission fits. In the sample with the highest Eu concentration, $x = 0.0475$, an enhanced broadening is observed in the $\alpha(\omega)$ spectrum for all temperatures either due to alloy fluctuations or due to the energetic neighborhood of the $4f$ Eu states ($S = \frac{7}{2}$) to the L_6^+ states. The hybridization of $4f$ Eu states with $5p^6$ valence-band states was already discussed

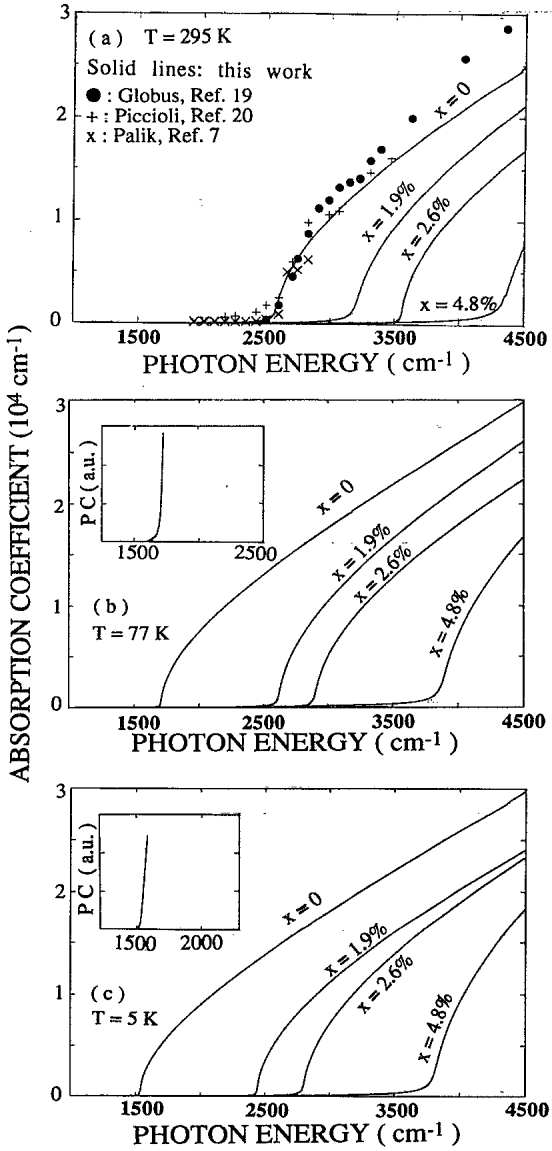

FIG. 3. Absorption coefficient $\alpha(\omega)$ for PbTe (sample A) and $Pb_{1-x}Eu_xTe$ (samples B, C, and D) at three temperatures: (a) 295 K, (b) 77 K, (c) 5 K. The insets in (b) and (c) show photoconductivity spectra (PC) which reproduce the onset of absorption in excellent agreement with fits to the transmission spectra.

in Ref. 33 for $Pb_{1-x}Eu_xTe$ ($x \geq 0.3$) and for EuTe.[36]

The index of refraction data $n(\omega)$ are plotted in Figs. 4(a)–4(c) for three temperatures 295, 77, and 5 K. The curves exhibit a maximum just above the onset of fundamental absorption. For PbTe [Figs. 4(a) and 4(b)] the index of refraction as published by Zemel, Jensen, and Schoolar,[18] Globus *et al.*,[19] and Piccioli, Beson, and Balkanski[20] (at 295 and 77 K) is compared to our data of epitaxial films. The positions of the energy gaps as calculated from the relation (Ref. 5)

$$\epsilon_g(x,T)=187\ \text{meV}+0.55\ \text{meV}\cdot T(\text{K})^2\frac{1-9x}{T(\text{K})+30}+x\cdot 6000\ \text{meV} \tag{20}$$

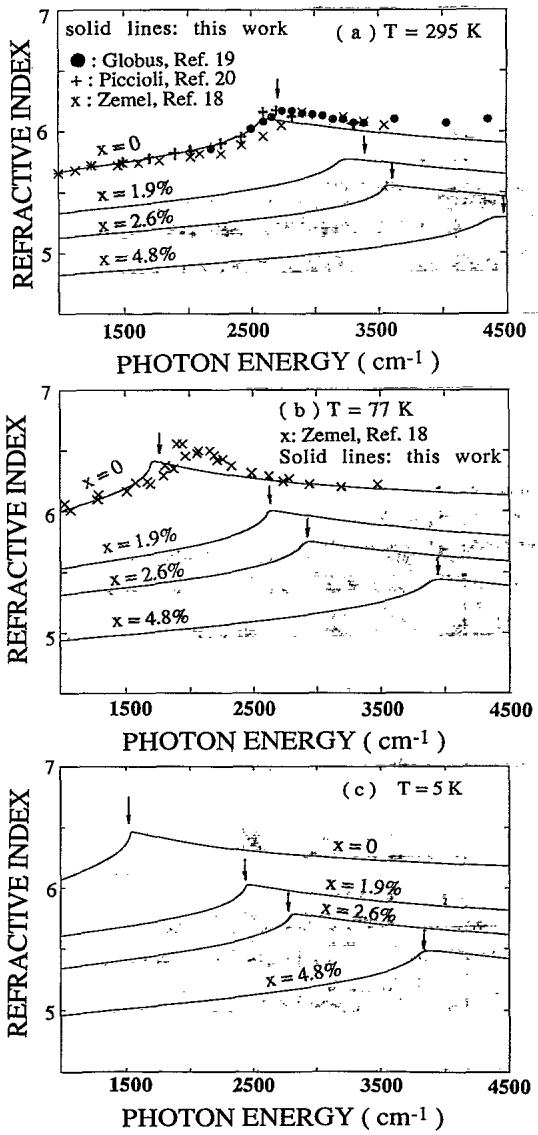

FIG. 4. Index of refraction $n(\omega)$ for PbTe (sample *A*) and $Pb_{1-x}Eu_xTe$ (samples *B*, *C*, and *D*) at three temperatures: (a) 295 K, (b) 77 K, (c) 5 K. Circles and crosses are previously published data for PbTe after Refs. 18 and 20. The arrows denote the positions of the fundamental absorption gap according to Partin's relation Eq. (20). Note the slight difference of these energetic positions in (a) from our results and from the published data.

are shown as arrows near the $n(\omega)$ maxima. The background index of refraction n_∞ (Table I) is decreasing for an increasing Eu content, as expected from the simultaneous increase of the energy gap.

By inspection of the parameter B in Table I, one notices a constant value for the oscillator strength except for sample D ($x=0.0475$), which in turn proves that the interband transitions are well described by PbTe-like momentum matrix elements $P_\parallel$ and $P_\perp$ as given by Eq. (5). In the two-band model they are taken as

$$\frac{2P_\perp^2}{m_0}=8.47\ \text{eV}\ ,\quad \frac{2P_\parallel^2}{m_0}=0.78\ \text{eV}\ , \tag{21}$$

which corresponds to masses $m_\perp^{e,h}=0.022m_0$, $m_\parallel^{e,h}=0.24m_0$ at $T=5$ K.

Since it is well known that the far bands also modify the band-edge effective masses of electrons and holes, Eq. (5), the values quoted in Eq. (21) do not correspond to those which are obtained from fits to magneto-optical experiments using both the exact two-band conduction-band–valence-band interaction and considering the effect of the far bands in the k^2 approximation.[11,32] For the calculation of the absorption coefficient, we modify the two-band parameters $P_\parallel$ and $P_\perp$ so as to result approximately in the proper mean electron and hole mass anisotropy and to also yield proper mean values of the transverse ($m_\perp$) and longitudinal ($m_\parallel$) effective masses. Up to about $x=5\%$ the band alignment of $Pb_{1-x}Eu_xTe$ does not change,[5] and consequently $P_\perp$ and $P_\parallel$ are assumed to be constant, i.e., independent of x. Using Eqs. (5) and (16) one calculates $B=2.91/\langle n\rangle$, in good agreement with the values of B in Table I obtained by our fits to the transmission data. The slight dependence of B on the Eu content is shown in Fig. 5 (the solid line is only a guide to the eye). At $x=0.0475$ the oscillator strength is discontinuously enhanced, presumably by the increase of

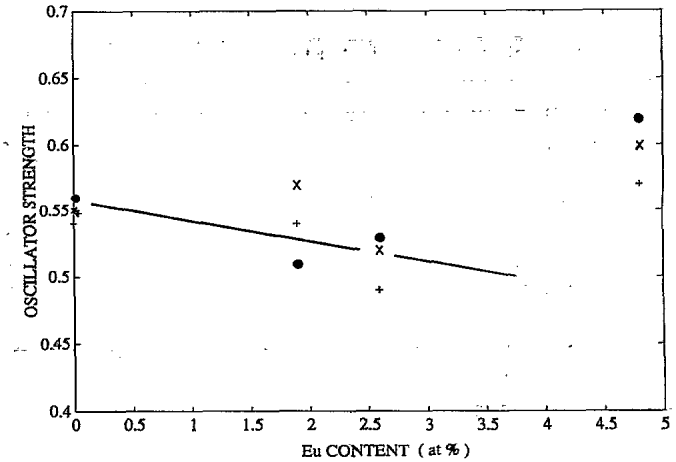

FIG. 5. Oscillator strength B according to Eq. (16) as a function of the Eu content. The interband momentum matrix elements are assumed to be those of PbTe for $x<0.0475$. For $x\geq 0.0475$ the oscillator strength is enhanced discontinuously, which comes from the interaction of band states with the $4f$-localized states of Eu atoms.

momentum matrix elements $P_{\parallel}$ and $P_{\perp}$ due to the interaction with the $4f$ Eu states.

Alloy broadening is important for $x > 0.0265$ at all temperatures. It is responsible for a smoother decay of the Fabry-Perot transmission maxima toward the fundamental absorption edge at a fixed energy gap. We believe that higher x content samples differ from our simple two-band model due to a beginning hybridization of the valence band with the $4f^7$ Eu energy levels, which also leads to the steplike enhancement of the oscillator strength for $x = 0.0475$.

The variation of the energy gap with the Eu content x in $Pb_{1-x}Eu_xTe$ is shown in Figs. 6(a) and 6(b) for three temperatures. The ϵ_g versus x relation derived from our fits is nearly linear. It is plotted in Fig. 6(b) and compared with that of Eq. (20) in Fig. 6(a).[5] Our data are only in good agreement with those of Partin,[5] Eq. (20), for $T = 5$ K. They deviate considerably for higher temperatures from Partin's relation, which holds for $Pb_{1-x}Eu_xSe_yTe_{1-x-y}$. Therefore, for $Pb_{1-x}Eu_xTe$ Eq. (20) is modified:

$$\epsilon_g(x,T) = 190 \text{ meV} + 0.51 \text{ meV} \cdot T(\text{K})^2 \frac{1-9.8x}{T(\text{K})+56} + x \cdot 5880 \text{ meV} \quad (22)$$

The ϵ_g versus x plots of Figs. 6(a) and 6(b) are the result

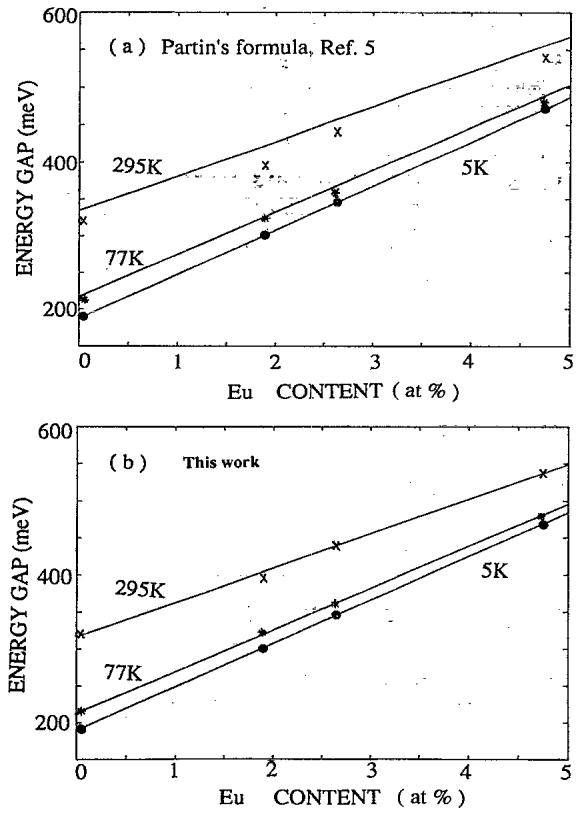

FIG. 6. Energy gap of $Pb_{1-x}Eu_xTe$ as a function of the Eu content for three temperatures. (a) Partin's formula Eq. (20) shows a slight difference (see the crosses) to the results of transmission measurements at 295 K. (b) Our modification to Eq. (22) gives a good agreement with the experiment at all temperatures.

of a search for a consistent set of band parameters (within the framework of a two-band model) for four samples and a wide temperature range. The excellent correspondence to Partin's formula at $T = 5$ K is not astonishing, since the T^2 prefactor in formula (22) becomes more and more negligible for $T \to 0$. Therefore, the x values originally taken from Partin's formula at $T = 5$ K are reliable starting parameters for the fits, but because of their validity at higher temperatures the second part of Partin's formula had to be modified accordingly with minor corrections of the other parts.

V. DISCUSSION AND SUMMARY

From the results of this work, one can conclude that the near-band-gap optical properties of IV-VI semiconductor epitaxial layers are consistently described by a simple two-band model, taking into account the full nonparabolicity according to the Dimmock model neglecting far-band contributions. The assumption of an energy-independent Lorentzian lifetime broadening (Γ) seems to be artificial, but is convenient in the sense that only one additional parameter enters into the calculations. However, there is also a physical reason to keep the broadening Γ finite for energies close to the band edge: since causality between extinction coefficient and index of refraction has to be maintained, the onset of absorption (α) with a discontinuous slope (neglecting any broadening at the band edge) would produce a singularity for the slope of the index of refraction near the absorption edge. Because such a singularity is unphysical, one has to avoid the discontinuous slope of α at $\epsilon = \epsilon_g$: undoped samples may exhibit residual "tail" states below the band edge (exponential Urbach tail). However, our samples are n type, and thus the tail states are occupied. Consequently, the onset of absorption, which starts not at zero but at a finite density of states, is discontinuous itself for $T \to 0$ with an even more dramatic influence on the index of refraction than for a discontinuous slope. The convolution of the density of states with a broadening function according to Eq. (12) keeps the slope of α continuous at $\epsilon = \epsilon_g$.

It is interesting to compare II-VI and IV-VI semiconductors of a similar narrow gap with each other: as stated by Herrmann and Rudolph,[21] $Hg_{0.796}Cd_{0.205}Te$ and PbTe behave differently in the dispersion of the index of refraction. Whereas the latter material exhibits a more or less pronounced maximum of $n(\omega)$ near ϵ_g, the former does not. An excitonic absorption at the leading edge of absorption does not ocur in narrow-gap semiconductors, particularly in PbTe, with its high static dielectric constant at low temperatures. Herrmann, Müller, and Melzer[22] conclude that the maximum in the index of refraction for the lead salts arises from the steeper absorption edge as compared to that of $Hg_{1-x}Cd_xTe$.

In our model calculations, a correct choice of a *single* broadening parameter Γ changes the maximum of the refractive index correspondingly to fit the transmission spectra both above and below the energy gap. The only remaining decision that has to be made is, is it sufficient to use a simple parabolic dispersion for $\epsilon(\mathbf{k})$, i.e., con-

stant combined density-of-state masses, or does a nonparabolic $\epsilon(\mathbf{k})$ dispersion have to be used for calculating $\alpha(\omega)$ and $n(\omega)$? As demonstrated in Fig. 1(a) for PbTe, the *nonparabolic* dispersion of energy bands *above* ϵ_g determines the position of Fabry-Perot interferences *below* ϵ_g in better agreement with the experimental data than the assumption of a parabolic $\epsilon(\mathbf{k})$ dispersion.

In Fig. 7 an attempt is made to fit the transmission spectrum of Fig. 1(a) by altering the parameters of the nonparabolic model accordingly to get a comparable fit using the parabolic approximation. The quality of the parabolic fit (Fig. 7) seems to be comparable to the nonparabolic one of Fig. 1(a). However, the optimized parameters for the parabolic approximation deviate appreciably from those obtained by theory: e.g., the oscillator strength B is fitted as 0.83 (theory: $B=0.513$), whereas the corresponding value of the nonparabolic fit is $B=0.054$, in excellent agreement with the theory. Thus, we conclude that the use of the parabolic two-band model leads to unphysical parameters. It also influences the behavior of the absorption coefficient above the band edge (see below, Fig. 9). By inspection of Figs. 1(a) and 7, it is obvious that the Fabry-Perot fringes, which are determined by the index of refraction below the fundamental absorption edge, are of different phases using the parabolic or nonparabolic model. The Kramers-Kronig relations are responsible for explaining this behavior: the correct dispersion $n(\omega)$, which crucially alters the observed distance between subsequent extrema in transmission both below and above the fundamental gap, is only obtained from the proper frequency dependence of $\alpha(\omega)$ *above* the energy gap.

Another crucial aspect in adopting the nonparabolic model is the extrapolation of $\kappa(\omega)$ to higher photon energies. Whereas $\kappa(\epsilon)\rightarrow 0$ for $\epsilon\rightarrow\infty$ in the parabolic case, $\kappa(\infty)=$const in the nonparabolic case, and accordingly $\alpha(\epsilon)$ diverges at high photon energies. As expected, the nonparabolic two-band model fails at too-high photon energies. In order to demonstrate the error in the refractive index obtained by Kramers-Kronig transformation due to an arbitrary high-frequency cutoff, we used for the upper cutoff wave-number limits the following values: $\bar{\omega}_c=5000$, 10 000, and 15 000 cm^{-1}. For this entire span of cutoff frequencies, the index of refraction above the band edge does not deviate by more than 5% from that, as shown in Fig. 8. This figure also demonstrates the influence of the lifetime broadening (Γ) on the dispersion of the index of refraction. The spectrum of the index of refraction neglecting broadening ($\Gamma=0$) is given in the figure as a dashed line. The infinite slope of $n(\Gamma=0)$ at $\epsilon=\epsilon_g$ is obvious, as discussed above. Broadening ($\Gamma\neq 0$) rounds off the $n(\epsilon_g)$ maximum.

Figures 9 and 10 show simulated spectra of the absorption coefficient and the index of refraction for PbTe at 295 K for the parabolic and nonparabolic case up to $\hbar\omega\approx 2\epsilon_g$. We would like to emphasize that previously published data[17–20] for $\alpha(\omega)$ and $n(\omega)$ for PbTe at $T=300$ K agree much better with the results of the nonparabolic model (solid curves) than for the two parabolic models (dashed and dashed-dotted curves). Using the same oscillator strength as for the nonparabolic approximation, the reduction to the parabolic limit yields a dependence with a drastic reduction of the absorption coefficient and of the peak index of refraction (dashed-dotted curves in Figs. 9 and 10). The corresponding transmission spectrum is that of Fig. 1(a) (dashed curve). If one enhances the oscillator strength beyond the value which is obtained by theory to $B=0.83$ instead of $B=0.54$ (dashed curves in Figs. 9 and 10), the absorption coefficient and the peak index of refraction can be brought to a closer agreement with the experiment (see

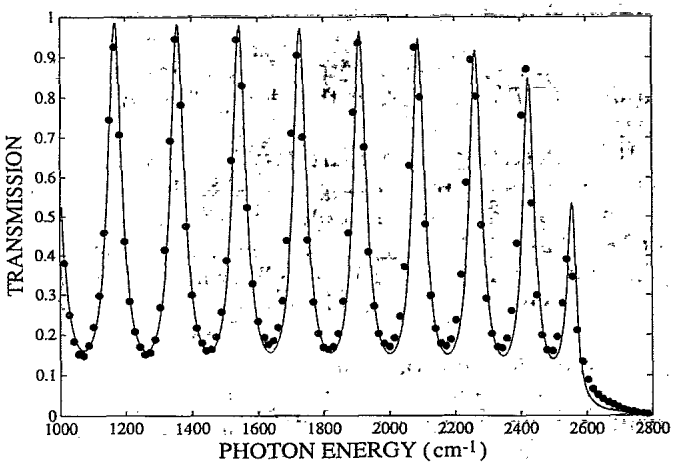

FIG. 7. Transmission of PbTe (sample A) at $T=295$ K, as compared to a *parabolic* two-band model (solid line). The model parameters were optimized correspondingly to fit the measured transmission spectrum (circles). As a result, the oscillator strength B has to be modified to $B=0.83$ in disagreement with theory ($B=0.513$). If the correct value were used in the parabolic limit, the calculated spectrum would deviate substantially from the measured one [see Fig. 1(a), dashed curve].

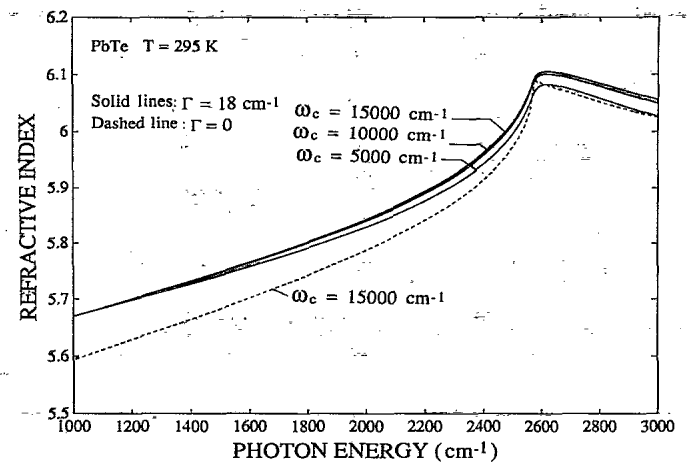

FIG. 8. Dispersion of the refractive index of PbTe (Sample A) at $T=295$ K above and below the fundamental energy gap using the nonparabolic two-band model and the Kramers-Kronig transformation. The influence of the chosen upper cutoff frequency (ω_c) on the Kramers-Kronig transformation is proved to be of minor importance. A finite broadening parameter (Γ) reduces the slope of $n(\omega)$ at $\hbar\omega=\epsilon_g$, which is infinite for $\Gamma=0$ (dashed curve).

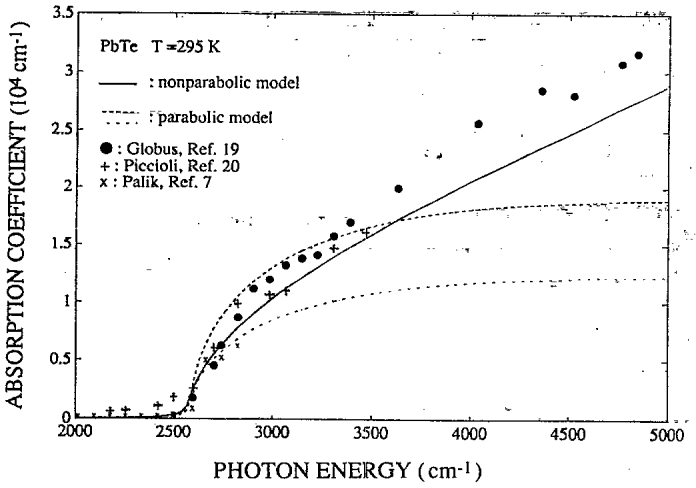

FIG. 9. Infuence of the chosen two-band model on the absorption coefficient $\alpha(\omega)$ for PbTe (sample A) at $T=295$ K. The *nonparabolic* model (solid curve) using the oscillator strength $B=0.54$ fits the published data according to Refs. 18–20 quite well. In the limit of a *parabolic* model using either the same $B=0.54$ (dashed-dotted curve) or fitting the data with an increased $B=0.83$ (dashed curve), strong deviations from the experimental values are noticed.

transmission spectrum, Fig. 7). However, the *slope* of $n(\omega)$ above ϵ_g deviates from the observations much more than that resulting from the nonparabolic model. These results essentially rule out the use of a parabolic model for $\epsilon(\mathbf{k})$ for the determination of both $\alpha(\omega)$ and $n(\omega)$. We have used a simple two-band model to account for nonparabolicity. From magneto-optical investigations it is well known that an extended model considering far-band contributions in the $\mathbf{k}^2$ approximation has to be used to describe the slight differences in electron and hole effective masses. The far-band contributions alter somewhat the energy-momentum relationship and consequently the proper dependence of $\alpha(\omega)$. These contributions were considered by Anderson[6] for the calculation of gain spectra for heterostructure IV-VI lasers. However, the influence of the broadening parameter Γ on $\alpha(\omega)$ and of the artificially chosen cutoff frequencies for the calculation of $n(\omega)$ on the calculated transmission spectrum is of comparable magnitude as the corrections to $\alpha(\omega)$ due to

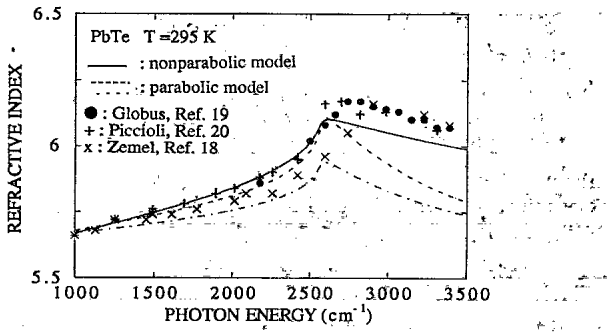

FIG. 10. Influence of the chosen two-band model on the dispersion of the refractive index of PbTe (sample A) at $T=295$ K. The various curves correspond to those of Fig. 9.

the far-band contributions in the energy-momentum relationship.

In summary, we have determined the optical constants of PbTe and $Pb_{1-x}Eu_xTe$ ($x \leq 0.0475$) epitaxial layers grown on insulating BaF_2 substrates below, across, and above the fundamental absorption edge. The thicknesses of the samples were chosen such as to observe a sufficient number of Fabry-Perot fringes in transmission below the fundamental gap. In these lead salts, which have an extraordinary high index of refraction ($n=4.75-6.2$), the influence of the carrier energy-momentum relationship *above* ϵ_g is even decisive for the magnitude and for the phase of the Fabry-Perot interferences observed in the transmission of the epitaxial layers *below* the energy gap. The absorption coefficient and index of refraction are presented for three temperatures (295, 77, and 5 K) as a function of photon energy. To our knowledge, the dispersion of the index of refraction for $Pb_{1-x}Eu_xTe$ at these temperatures is determined for the first time. The energy of the forbidden gap at the L point of the Brillouin zone varies almost linearly with the Eu content, at least for our concentration $x \leq 0.0475$. However, hybridization of $4f$ Eu states with $5p^6$ PbTe valence-band states has some spurious influence on the oscillator strength of interband transitions and on the linewidth broadening already for an Eu content of $x=0.0475$. The M_0 critical-point transition at the fundamental absorption edge is treated in the framework of a strict nonparabolic two-band $\mathbf{k}\cdot\mathbf{p}$ model, which restricts the number of parameters for fitting the transmission spectra to four: energy gap, oscillator strength, linewidth broadening, and background index of refraction (the latter can be taken also from the fits to absorption spectra in the vicinity of critical points at higher energies). Thus we believe that the model presented is rather simple, unambiguous, and does not violate causality.

ACKNOWLEDGMENTS

We thank Professor K. Herrmann (Humboldt-Universität Berlin) for some clarifying discussions about the dispersion of the index of refraction in PbTe above the fundamental absorption edge and the broadening function dependence on the Eu content in $Pb_{1-x}Eu_xTe$. We thank also T. Dietl and Professor P. Grosse for stimulating discussions, and M. Seto for providing us with the numerical integration program. The work was supported by the Österreichischer Fonds zur Förderung der wissenschaftlichen Forschung under Projects P8250 and P8446.

APPENDIX A: JOINT DENSITY OF STATES ACCORDING TO A NONPARABOLIC TWO-BAND MODEL

At the L point of the Brillouin zone of PbTe (Fig. 11), the surfaces of constant energy are ellipsoids of revolution oriented with the principal $\parallel$ axis along [111] and $\perp$ axis perpendicular to [111]. The curvatures are given by the squares of the momentum interband matrix elements $P_\parallel^2$ and $P_\perp^2$. In a strict two-band model neglecting far-band contributions, the $\mathbf{k}\cdot\mathbf{p}$ approximation near the L

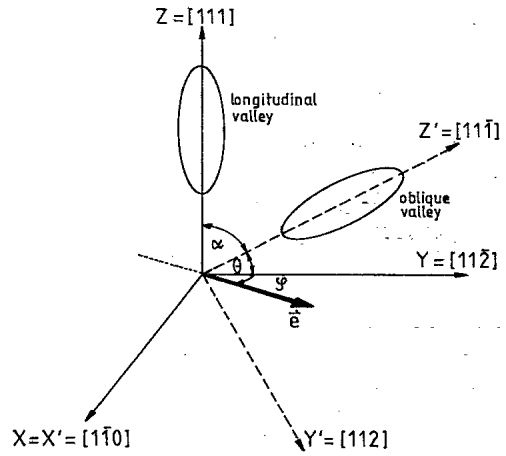

FIG. 11. Coordinate frames for the constant-energy ellipsoids of PbTe near the L point of the Brillouin zone: Unprimed system for the longitudinal valley, primed system for the oblique valley. The incident light is along the z direction, which is the growth direction of the epitaxial layers. Its polarization vector is denoted by $\mathbf{e}$, which is finally averaged over $0 \leq \varphi \leq 2\pi$ for interaction of unpolarized light.

point gives the following mirrorlike energy-momentum dispersion relations for the conduction (c) and the valence (v) bands:

$$\epsilon_c(\mathbf{k})=\frac{\hbar^2}{2m_0}\mathbf{k}^2+\frac{1}{2m_0}[4\hbar^2P_\perp^2(k_x^2+k_y^2)+4\hbar^2P_\parallel^2k_z^2 + m_0^2\epsilon_g^2]^{1/2} , \tag{A1}$$

$$\epsilon_v(\mathbf{k})=\frac{\hbar^2}{2m_0}\mathbf{k}^2-\frac{1}{2m_0}[4\hbar^2P_\perp^2(k_x^2+k_y^2)+4\hbar^2P_\parallel^2k_z^2 + m_0^2\epsilon_g^2]^{1/2} . \tag{A2}$$

The transition energy between the valence and conduction bands corresponds to the photon energy (obeying momentum conservation $\mathbf{k}_c=\mathbf{k}_v=\mathbf{k}$):

$$\epsilon=\hbar\omega=\epsilon_c(\mathbf{k})-\epsilon_v(\mathbf{k}) =\frac{1}{m_0}(4\hbar^2P_\perp^2k_\perp^2+4\hbar^2P_\parallel^2k_z^2+m_0^2\epsilon_g^2)^{1/2} . \tag{A3}$$

This can be rewritten as

$$\frac{k_\perp^2}{a^2}+\frac{k_z^2}{b^2}=1 , \tag{A4}$$

which reflects the ellipsoidal shape of the constant energy surface in $\mathbf{k}$ space with principal axes a and b:

$$a^2=\frac{m_0^2}{4\hbar^2P_\perp^2}(\epsilon^2-\epsilon_g^2) , \tag{A5}$$

$$b^2=\frac{m_0^2}{4\hbar^2P_\parallel^2}(\epsilon^2-\epsilon_g^2) . \tag{A6}$$

The quotient a^2/b^2 corresponds to the mass anisotropy of band-edge masses $m_\perp/m_\parallel$ at the L point of the Brillouin zone. The differential volume $dV_\mathbf{k}$ in $\mathbf{k}$ space between adjacent energy surfaces ϵ and $\epsilon+d\epsilon$ can be calculated by differentiating the ellipsoid volume $V_\mathbf{k}=(\frac{4}{3})\pi a^2b$:

$$dV_\mathbf{k}=\frac{\pi m_0^3}{2\hbar^3P_\perp^2P_\parallel}\epsilon(\epsilon^2-\epsilon_g^2)^{1/2}d\epsilon . \tag{A7}$$

The number of states within $dV_\mathbf{k}$ (the phase-space cell is $8\pi^3/V_r$, V_r the crystal volume) can be expressed by the joint density of states $J_{cv}(\epsilon)$:

$$dN(\epsilon)=2\frac{V_r}{8\pi^3}dV_\mathbf{k}=V_rJ_{cv}(\epsilon)d\epsilon . \tag{A8}$$

If one inserts Eq. (A7) into Eq. (A8), the joint density of states $J_{cv}(\epsilon)$ becomes

$$J_{cv}(\epsilon)=\frac{m_0^3}{8\pi^2\hbar^3P_\perp^2P_\parallel}\epsilon(\epsilon^2-\epsilon_g^2)^{1/2} . \tag{A9}$$

It should be noted that Eq. (A9) holds only for mirrorlike nonparabolic energy bands in the strict two-band approximation. If the contribution of far bands is included up to the order of $\mathbf{k}^2$, then the "effective" momentum matrix elements $P_\parallel$ and $P_\perp$ have to be modified correspondingly as traditionally used in the literature.[11,32]

APPENDIX B: THE EVALUATION OF THE INTERBAND MATRIX ELEMENTS

The IV-VI semiconductors have their fundamental energy gap at the L point of the Brillouin zone. From this reason their band-edge wave functions are valley degenerate. The basis functions at the L point of the Brillouin zone in the notation of Mitchell and Wallis[32] are related to our notation by

$$|L_{62}^-\alpha\rangle=-\sin\Theta^-|Z\uparrow\rangle-\cos\Theta^-|X_+\downarrow\rangle=|C\uparrow\rangle , \tag{B1}$$

$$|L_{62}^-\beta\rangle=\sin\Theta^-|Z\downarrow\rangle-\cos\Theta^-|X_-\uparrow\rangle=|C\downarrow\rangle , \tag{B2}$$

$$|L_{61}^+\alpha\rangle=i\cos\Theta^+|R\uparrow\rangle+\sin\Theta^+|S_+\downarrow\rangle=|V\uparrow\rangle , \tag{B3}$$

$$|L_{61}^+\beta\rangle=i\cos\Theta^+|R\downarrow\rangle+\sin\Theta^+|S_-\uparrow\rangle=|V\downarrow\rangle . \tag{B4}$$

$|C\uparrow\rangle,|C\downarrow\rangle,|V\uparrow\rangle,|V\downarrow\rangle$ denote conduction- and valence-band spin-up and spin-down states in our notation. The other symbols are convenient for the L-point symmetry (D_{3d}) and are explained in Ref. 32. We evaluate the interband transition matrix elements for two specific valleys of a IV-VI semiconductor epitaxial layer with surface normal along [111]: (i) the longitudinal valley oriented along the unprimed z axis parallel to [111], (ii) the oblique valley oriented along the z' axis parallel to [11$\bar{1}$]. The light is incident in the [111] direction with polarization vector $\mathbf{e}$ in the x,y plane of the unprimed coordinate frame (Fig. 11). We shall average finally over all azimuth angles φ of the polarization vector $\mathbf{e}$ to obtain the transition matrix elements for unpolarized light. Without specifying a certain polarization direction, the remaining oblique valleys oriented along [1$\bar{1}$1] and [$\bar{1}$11] have the same interband transition probability as the [11$\bar{1}$] oblique valley. $\alpha=70.53°$ is the angle between [111] and [11$\bar{1}$], and θ is its complement to 90°.

The basis functions of Eqs. (B1)–(B4) are correct only in the individual coordinate frame of a certain valley (possessing a longitudinal and transverse principal axis). Therefore, the polarization vector has to be projected onto the coordinate axes of the corresponding valley: (i) for the longitudinal valley

$$\mathbf{e}=(e_x,e_y,e_z)=(\sin\varphi,\cos\varphi,0); \tag{B5}$$

(ii) for the transverse valley,

$$\mathbf{e}'=(e_x',e_y',e_z')=(\sin\varphi,\cos\alpha\cos\varphi,\sin\alpha\cos\varphi)$$
$$=(\sin\varphi,\tfrac{1}{3}\cos\varphi,\sqrt{8}/3\cos\varphi)\ . \tag{B6}$$

By selecting the proper coordinate frame, the square of the interband matrix element for both valleys is expressed by the same formula (if $\mathbf{e}$ of the longitudinal valley is replaced by $\mathbf{e}'$ for the oblique valley):

$$|\langle C|\mathbf{e}\cdot\mathbf{p}_{cv}(0)|V\rangle|^2=\sum_{i,j=\uparrow\downarrow}|\langle C_i|\mathbf{e}\cdot\mathbf{p}_{cv}(0)|V_j\rangle|^2\ . \tag{B7}$$

From Table I of Ref. 32, the set of matrix elements can be evaluated in the following way:

$$\langle C\uparrow|\mathbf{e}\cdot\mathbf{p}_{cv}(0)|V\uparrow\rangle=P_{\parallel}e_z\ , \tag{B8}$$

$$\langle C\uparrow|\mathbf{e}\cdot\mathbf{p}_{cv}(0)|V\downarrow\rangle=P_{\perp}(e_x+ie_y)\ , \tag{B9}$$

$$\langle C\downarrow|\mathbf{e}\cdot\mathbf{p}_{cv}(0)|V\uparrow\rangle=P_{\perp}(e_x-ie_y)\ , \tag{B10}$$

$$\langle C\downarrow|\mathbf{e}\cdot\mathbf{p}_{cv}(0)|V\downarrow\rangle=-P_{\parallel}e_z\ . \tag{B11}$$

Replacement of e_x, e_y, and e_z by the primed expressions of Eq. (B6) yields the corresponding transition matrix elements for the oblique valley. The total matrix element is the sum over the longitudinal valley and three times over the oblique valley (in the specific case of unpolarized excitation), which can be evaluated in a straightforward manner using Eqs. (B8)–(B11) and by selecting the corresponding type of valleys:

$$\langle|\mathbf{e}\cdot\mathbf{p}_{cv}(0)|^2\rangle_{\text{valleys}}=\sum_{i,j=\uparrow\downarrow}^{\text{long}}|\langle C_i|\mathbf{e}\cdot\mathbf{p}_{cv}(0)|V_j\rangle|^2+3\sum_{i,j=\uparrow\downarrow}^{\text{oblique}}|\langle C_i|\mathbf{e}\cdot\mathbf{p}_{cv}(0)|V_j\rangle|^2$$
$$=2P_{\perp}^2+3(\tfrac{8}{9}P_{\parallel}^2+\tfrac{10}{9}P_{\perp}^2)=\tfrac{8}{3}(2P_{\perp}^2+P_{\parallel}^2)\ . \tag{B12}$$

[1]Ch. C. Kim, J. W. Garland, H. Abad, and P. M. Raccah, Phys. Rev. B **45**, 11 749 (1992).

[2]A. R. Forouhi and I. Bloomer, in *Handbook of Optical Constants of Solids II,* edited by E. D. Palik (Academic, Boston, 1991), p. 151.

[3]J. D. Klein, A. Yen, and S. F. Cogan, J. Appl. Phys. **68**, 1825 (1990).

[4]P. Grosse and V. Offermann, Appl. Phys. A **52**, 138 (1991).

[5]D. L. Partin, IEEE J. Quantum Electron. **QE-24**, 1716 (1988).

[6]W. A. Anderson, IEEE J. Quantum Electron. **QE-13**, 532 (1977).

[7]For PbS, PbSe, and PbTe, see references in E. D. Palik, *Handbook of Optical Constants of Solids* (Academic, Orlando, 1985), pp. 528, 517, and 535.

[8]W. A. Anderson, Infrared Phys. **20**, 363 (1980).

[9]D. L. Partin, in *Semiconductors and Semimetals,* edited by R. K. Williardson and A. C. Beer (Academic, Boston, 1991), Vol. 33, p. 311.

[10]G. Bauer and H. Pascher, in *Diluted Magnetic Semiconductors,* edited by M. Jain (World Scientific, Singapore, 1991), p. 340.

[11]G. Bauer, H. Pascher, and W. Zawadzki, Semicond. Sci. Technol. **7**, 703 (1992).

[12]Z. Feit, D. Kostyk, R. J. Woods, and P. Mak, Appl. Phys. Lett. **58**, 343 (1991).

[13]D. L. Partin, J. Heremans, C. M. Thrush, L. Green, and C. H. Olk, Phys. Rev. B **38**, 3549 (1988).

[14]A. Lopez-Otero, Thin Solid Films **49**, 1 (1978).

[15]A. K. Walton and T. S. Moss, Proc. Phys. Soc. **81**, 509 (1963).

[16]G. Galeczki, Infrared Phys. **31**, 215 (1991).

[17]S. L. McCarthy, W. H. Weber, and M. Mikkor, J. Appl. Phys. **45**, 4907 (1974).

[18]J. N. Zemel, J. D. Jensen, and R. B. Schoolar, Phys. Rev. **140A**, 330 (1965).

[19]T. R. Globus, B. L. Gelmont, K. I. Geiman, V. A. Kondrashov, and A. V. Matveenko, Zh. Eksp. Teor. Fiz. **80**, 1926 (1981) [Sov. Phys.—JETP **53**, 1000 (1981)].

[20]N. Piccioli, J. M. Beson, and M. Balkanski, J. Phys. Chem. Solids **35**, 971 (1974).

[21]K. H. Herrmann and A. F. Rudolph, Infrared Phys. **33**, 63 (1992).

[22]K. H. Herrmann, U. Müller, and V. Melzer (unpublished).

[23]G. Nimtz and B. Schlicht, in *Narrow Gap Semiconductors,* edited by G. Höhler, Springer Tracts in Modern Physics Vol. 98 (Springer, Berlin, 1983).

[24]M. M. El-Ocker, F. Sharaf, H. M. Talaat, F. Metawe, and M. A. El-Sherbiny, Solid State Commun. **76**, 1293 (1990).

[25]M. Cardona and D. L. Greenaway, Phys. Rev. **133A**, 1685 (1964).

[26]A. W. Verleur, J. Opt. Soc. Am. **58**, 1356 (1968).

[27]K. Q. Zhang and Y. Yen, Appl. Opt. **28**, 2929 (1989).

[28]G. Bauer and H. Clemens, Semicond. Sci. Technol. **5**, S122 (1990).

[29]A. R. Forouhi and I. Bloomer, Phys. Rev. B **38**, 1865 (1988).

[30]G. Springholz and G. Bauer, Appl. Phys. Lett. **60**, 1600 (1992).

[31]J. O. Dimmock and G. B. Wright, Phys. Rev. **135A**, 821 (1964).

[32]D. L. Mitchell and R. F. Wallis, Phys. Rev. **151**, 581 (1966).

[33]W. C. Goltsos, A. V. Nurmikko, and D. L. Partin, *Solid State*

Commun. **59**, 183 (1986).
[34]H.-S. Cho and P. R. Prucnal, Phys. Rev. B **39**, 11 150 (1989).
[35]A. F. Terzis, X. C. Liu, A. Petrou, B. D. McCombe, M. Dutta, H. Shen, D. D. Smith, M. W. Cole, M. Taysing-Lara, and P. G. Newman, J. Appl. Phys. **67**, 2501 (1990).
[36]P. Wachter, in *Handbook on the Physics of Rare Earths*, edited by K. A. Gschneidner and L. Eyring (North-Holland, Amsterdam, 1979), p. 507.